This document is published in:

L. Bolzoni, E.M. Ruiz-Navas, E. Gordo. Influence of Sintering Parameters on the Properties of Powder Metallurgy Ti-3Al-2.5V Alloy. *Materials Characterization* vol. 84, (2013), pp. 48-57.

DOI: http://dx.doi.org/10.1016/j.matchar.2013.07.009

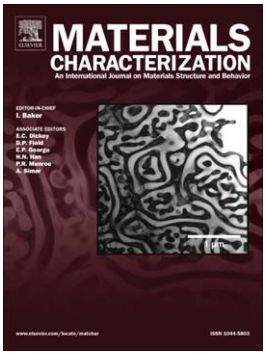

Influence of Sintering Parameters on the Properties of Powder Metallurgy Ti-3Al-2.5V Alloy

L. Bolzoni, E.M. Ruiz-Navas, E. Gordo

PII: S1044-5803(13)00210-6
DOI: doi: 10.1016/j.matchar.2013.07.009
Reference: MTL 7381

To appear in: *Materials Characterization*

Received date: 19 February 2013
Revised date: 6 June 2013
Accepted date: 5 July 2013

Please cite this article as: Bolzoni L, Ruiz-Navas EM, Gordo E, Influence of Sintering Parameters on the Properties of Powder Metallurgy Ti-3Al-2.5V Alloy, *Materials Characterization* (2013), doi: 10.1016/j.matchar.2013.07.009

Influence of Sintering Parameters on the Properties of Powder Metallurgy Ti-3Al-2.5V Alloy

L. Bolzoni[1,*], E.M. Ruiz-Navas[2] and E. Gordo[3]

Departamento de Ciencia e Ingeniería de Materiales e Ingeniería Química

Universidad Carlos III de Madrid

Avda. de la Universidad, 30, 28911 Leganés (Madrid), Spain

Tel: +34916249482, Fax: +34916249430

e-mail: [1]bolzoni.leandro@gmail.com, [2]emruiz@ing.uc3m.es, [3]elena.gordo@uc3m.es

Abstract

The processing of near net shape Ti-3Al-2.5V components using the conventional pressing and sintering route is addressed in this study. The Ti-3Al-2.5V starting powder was obtained considering both the blending elemental and the master alloy addition methods. The powders were uniaxially pressed and sintered in a high-vacuum furnace under various temperature-time combinations. The influence of the processing parameters on the relative density, microstructural features, amount of interstitials, mechanical behaviour, thermal conductivity and electrical resistivity of the sintered materials was evaluated. It was found that the relative density of the samples increases with processing temperature and time, and almost fully dense materials were obtained. The mechanical performance of the Ti-3Al-2.5V improves due to the reduction of the residual porosity and are, generally, of the same order of magnitude of those required for titanium biomedical products. Furthermore, the temperatures-times selected permit to obtain thermal and electrical properties similar to the wrought alloy.

Keywords: titanium alloys, Ti-3Al-2.5V, powder metallurgy (PM), flexural properties, thermal conductivity, electrical resistivity

1. Introduction

Among common metals, titanium provides the highest ratio between strength and density, it maintains good resistance at relatives high temperatures, it has superior corrosion resistance in many various critical environments and very good biocompatibility. Titanium and its alloys are, therefore, ideal materials for diverse kind of industries due to the unique combination of lightness and properties that they provide. However, the employment of titanium is far less widespread with respect to other structural metals (i.e. steel or aluminium). Exceptions are limited to high performing industries like aerospace and biomedical applications. This limitation derives from the high extraction and production costs of titanium [1-3]. Among the various titanium alloys, the Ti-3Al-2.5V alloy was originally thought to be used for hydraulic and fuel structures in conventional airplanes. Nevertheless, recently this alloy has also been considered to fabricate biomedical and dental implants as well as tools for diverse spots (e.g. golf or baseball). The Ti-3Al-2.5V alloy is a super-α titanium alloy due to the presence of both α and β stabilisers and it has superior strength with respect to unalloyed titanium [3]. Powder metallurgy (PM) techniques are near net shape or net shape processes and, thus, offer important advantages in terms of material yield and number of production stages [4]. These aspect should reflect on the reduction of the fabrication costs of titanium products. Depending on the processed used to fabricate the powder, pre-alloyed (PA) and blending elemental (BE) titanium powder are normally available. The use of master alloys (MA) is a modification of the BE powders and it has been identified has the less expensive method to produce titanium alloys with both classical or novel compositions [5].

In the 1980´s, many investigations were done about the processing of titanium by means of PM techniques using titanium sponge powders [6-8]. The main drawback of using these powders is that the residual chlorides left from the extraction process fill the porosity with gas during sintering. At present, irregular titanium powders obtained by the hydride-de-hydride

(HDH) process can be found in the market. Thanks to their features, these powders can be used in the pressing and sintering route avoiding the drawback of the chlorides as in increasing number of publication demonstrates [9-13].

In this work the processing of Ti-3Al-2.5V components by combining the employment of the conventional pressing and sintering PM route and a HDH unalloyed titanium powder as starting material is studied. Two ways of adding the alloying elements are considered and the results obtained are compared to highlight potential differences. The influence of the processing parameters on the physical properties, amount of interstitials and mechanical behaviour is studied and correlated with microstructural features obtained. Finally, the thermal conductivity and the electrical resistivity of the PM titanium materials are measured to fulfil the lack of data available in the literature.

2. Experimental Procedure

A HDH unalloyed titanium powder and an Al-V master alloy from GfE GmbH and a HDH pre-alloyed Ti-6Al-4V powder from SeJong Materials were acquired. By conventional mixing of these powders, the Ti-3Al-2.5V alloy powder was fabricated. Precisely, Ti32-BE derives by the mixing of the HDH unalloyed titanium powder with the pre-alloyed Ti-6Al-4V powder whilst Ti32-MA is fabricated by mixing titanium and the Al-V master alloy [14].

The morphology, particle size and amount of interstitials of the Ti32-BE and Ti32-MA powders are reported in Table 1.

From Table 1, both powders have irregular morphology, similar mean particle size, however Ti32-MA has relative bigger particle size with respect to Ti32-BE. This aspect could influence the densification of the green samples and the mechanical properties because a bigger particle size usually leads to coarser microstructural features. On the contrary, a powder with a finer particle size has greater surface area, which enhances the densification; however it also has a greater amount of oxygen adsorbed onto the surface of the powder

particles. Actually, from the data shown in Table 1, the amount of oxygen is greater for the Ti32-BE powder.

Three points bending test samples (ASTM-B528) were pressed with the starting Ti-3Al-2.5V powders using an applied pressure of 700 MPa. However, on the results of a previous work [14], the pressure was reduced 300 MPa to prevent their delamination in the case of Ti32-BE samples. The difference in applied pressure influences the level of green density and, consequently, the densification during sintering. Nevertheless, it permits to study the reliability of the uniaxial pressing method. The sintering of the green specimens was carried out batch-by-batch in a high-vacuum furnace (minimum 10^{-5} mbar) and using heating and cooling rates of 5ºC/min. The sintering temperature window was 1250-1350ºC in combination with 2 hours and 4 hours as processing time. The volume variation induced by sintering was calculated by means of the dimensions (length, width and thickness) of the green and sintered samples. The relative density (ρ_{rel}) of the sintered specimens was calculated by the ratio between the density value obtained by water displacement measurements and the values (ρ) of the wrought Ti-3Al-2.5V alloy (4.48 g/cm^3) [3]. The phenomena that govern the sintering step were quantified by means of the densification parameter (Ψ), which was calculated using equation 1:

$$\Psi = \frac{\rho_{rel} - \rho_g}{\rho - \rho_g} * 100[\%] \qquad \text{(Eq. 1)}$$

where ρ_g is the green density of the samples.

The samples were analysed using the typical metallography (silicon-carbide papers grinding and silica-gel polishing), etching with Kroll reagent and an Olympus-GX71 microscope. The amounts of interstitials were measured by means of an appositely calibrated LECO TC-500 analyser using the ASTM-E1409 (oxygen) and the ASTM-E1937 (nitrogen) standards.

Vickers hardness measurements were performed in a Wilson-Wolpert DIGI-TESTOR 930 machine using a load of 30 kg. Flexural properties of the specimens were measured by means of a MicroTest three points bending test machine on the base of the ASTM-B528 standard. The values of the mechanical properties are presented as average and standard deviation obtained from three specimens. For the elastic limit, the off-set method was used because the samples showed plastic deformation before rupture. The study of the rupture surface of the specimens was done using a Philips-XL30 SEM which was also used to analyse the distribution and the alloying elements by EDS analysis.

The thermal conductivity at room temperature (k) of the sintered specimens was calculated using equation 2:

$$k = \alpha \cdot \rho_{rel} \cdot C_p \qquad \text{(Eq. 2)}$$

where: α is the thermal diffusivity, ρ_{rel} is the relative density of each sample and C_p is the specific heat capacity at constant pressure. A Netzsch LFA-447 Nanoflash equipment was used to determine the thermal diffusivity of the samples. The results of electrical conductivity measurements by means of the van der Pauw method [15, 16] were used to obtained the electrical resistivity at room temperature values. Finally, the samples sintered at 1250ºC-2hours were used to measure the thermal conductivity as a function of the increment of the temperature. Because also the specific heat capacity at constant pressure used to determine the thermal conductivity varies with the temperature, its variation was calculated using equation 3, which is suitable for α titanium [3]:

$$C_p = 669 - (0.037188 \cdot T) - (1.080 \cdot 10^7 \cdot T^{-2}) \qquad \text{(Eq. 3)}$$

T: temperature in Kelvin.

The thermal conductivity values calculated with the corrected C_p values were compared with the values obtained by the measurements and the data available in the literature.

3. Results and Discussion

3.1 Volume variation, densification and relative density of sintered materials

As already stated in the experimental procedure, Ti32-BE specimens were uniaxially pressed at 300 MPa whereas Ti32-MA specimens at 700 MPa. Consequently, the mean green density of Ti32-BE components, which is equal to 69.00% ± 0.75%, is lower with respect to that of the Ti32-MA samples, which is 86.64% ± 0.24%. It is expected that the lower the pressure applied to press the components, the higher the densification and the contraction of the specimens. The volume variation experienced by the samples is graphed as a function of the sintering parameters in Figure 1.

From Figure 1, the variation of the dimension of the specimens during the sintering results in shrinkage where this contraction is much more marked for Ti32-BE specimens. In particular, Ti32-BE samples have a mean shrinkage of approximately 25% where these values increases a little with the sintering temperature. In opposition, the time does not influence significantly the contraction of the components as much as the temperature does because samples sintered at the same temperature but with diverse dwell time show by the same shrinkage. Ti32-MA specimens show exactly the same behaviour with processing time and temperature; however the average shrinkage is about 11% due to the greater green density of the samples.

The densification experienced by the specimens during sintering is graphed as a function of the sintering conditions in Figure 2.

The densification of the samples (Figure 2) increases along with the temperature for both powders with the exception of the Ti32-MA powder sintered at 1350ºC during 4 hours whose densification is similar to that of samples sintered at 1300ºC for 4 hours. Moreover, the

densification of Ti32-MA is always higher with respect to Ti32-BE. Since the value of the density of the wrought alloy used to calculate the densification is the same and supposing that the two powders reach the same relative density, Ti32-BE should have a higher densification. Therefore, since Ti32-BE has a lower densification, Ti32-MA would reach higher final relative density.

The variation of the relative density of the samples with the processing conditions is plotted in Figure 3.

Independently of the method used to fabricate the powder and of the compaction pressure employed, the relative density of Ti32-BE and Ti32-MA components increases with the sintering temperature and it is a little bit higher for longer processing time (Figure 3). In one side, in the case of the Ti32-BE samples the increment of the relative density is more marked when increasing the sintering temperature from 1250ºC to 1300ºC, approximately 0.8%, than from 1300ºC to 1350ºC (roughly -0.1%). Furthermore, the increment of the dwell time seems to have the same effect independently of the temperature because the average increment is about 0.7%. In the other side, in the case of the Ti32-MA samples the increment of the sintering temperature seems to be more effective than the increasing the processing time in order to achieve high relative density values. In particular, the increment of the sintering temperature of 50ºC leads to a mean increment of 0.4% in relative density whilst the longer time produces an increment of 0.2%. By the comparison of the behaviour of Ti32-BE and Ti32-MA specimens, these last always reach higher relative density than Ti32-BE specimens. The final lower relative density of Ti32-BE components shown in Figure 3 compared to Ti32-MAsamples is primarily due to the lower compaction pressure (300 MPa) applied to consolidate the specimens which results in a lower green density. The relative density values shown in Figure 3 are similar to those available in the literature for PM titanium alloys [17-19].

3.2 Microstructural analysis of sintered materials

Figure 4 shows representative micrographs of the development of the microstructure and of the porosity of both materials.

From the micrograph presented in Figure 4, the increasing of the sintering temperature and of the processing time leads to a reduction of the porosity, which primary isolated and spherical, in agreement with the relative density data (Figure 3). This behaviour is valid for both Ti32-BE and Ti32-MA samples and, therefore, it is independent form the method used to fabricate the powder. From Figure 4, it can be also seen that α grains and α+β lamellae are the micro-constituents of the Ti32-BE and Ti32-MA samples because they were slow cooled from above the β-transus. Furthermore, it seems that the α phase grows with the temperature and the lamellae get bigger, being this behaviour more pronounced for longer time. Moreover, the lamellae of Ti32-MA specimens seem to be finer than those of Ti32-BE which is due to the combined effect of the smaller particle size of the Ti32-BE powder and the greater amount of thermal energy used to homogenise the alloying elements for the Ti32-MA samples. Therefore, this leads to the formation to a somewhat coarser microstructure in the components made out from the Ti32-MA powder with respect to those obtained starting from Ti32-BE. It is remarkable that the microstructures of both Ti32-BE and Ti32-MA specimens are homogeneous, as proved by EDS analysis, and no undissolved alloying element particles are present.

3.3 Amount of interstitials of sintered materials

The results of the amount of interstitials (oxygen and nitrogen) measured on sintered samples are presented in Table 2.

From Table 2, the amount of oxygen increases with the increment of the sintering temperature and it is, generally, relatively higher for longer processing time. In particular, the oxygen of the Ti32-BE specimens varies between 0.40 wt.% and 0.50 wt.% whereas in the case of the

Ti32-MA samples increases from 0.34 wt.% to a maximum value of 0.40 wt.% at the highest sintering temperature considered. The picks up of oxygen with respect to the initial content of the powder (Table 1) will influence the mechanical behaviour [20-22]. The increment of oxygen derives from various aspects such as handling and inwards diffusion of the elements adsorbed onto the powder particle. Regarding the nitrogen data of Table 2, the amount measured in the sintered specimens is quite similar to that of the starting powder and the difference between Ti32-BE and Ti32-MA is almost insignificant. Generally, the mean value of nitrogen for all the sintering conditions, and independently of the powder production route, is about 0.02 wt.% and, therefore, lower than the maximum allowed (0.03 wt.% [3]).

3.4 Hardness of sintered materials

The results of Vickers hardness measured in the cross sections of the specimens are presented in Figure 5.

Generally, the hardness of sintered Ti-3Al-2.5V titanium alloy (Figure 5) increases with the sintering temperature and time due to the increment of the relative density or, in turns, the reduction of the residual porosity. More in detail, in the case of the Ti32-BE samples the greatest increment is obtained when increasing the sintering temperature from 1300ºC to 1350ºC rather than 1250ºC to 1300ºC due to the greater increment of interstitial elements dissolved by the materials at these processing temperatures. In the case of the Ti32-MA specimens, the materials become harder with the increment of both the processing parameters and the longer time has the same effect, an increment of approximately 15 HV30, than increasing the sintering temperature in 50ºC. Normally, the values obtained for Ti32-MA samples are higher compared to those of the Ti32-BE specimens and this is in agreement with the density values (Figure 3). However, the difference is mitigated and becomes somewhat lower with the increment of the sintering temperature due to the increment of oxygen of the Ti32-BE samples. Depending on the heat treatment, wrought Ti-3Al-2.5V has hardness

between 220 HV and 300 HV (mean value of 267 HV in the annealed state) [3]. From the data displayed in Figure 5, apart from the Ti32-BE samples sintered at 1250ºC-2h, the hardness of the PM Ti-3Al-2.5V alloys studied equals or overcomes that of wrought material despite the residual porosity (3-6%)0. The behaviour is due the combined effect of the higher amount of interstitial elements that both Ti32-BE and Ti32-MA components have with respect to the wrought alloy and the, normally, finer microstructural features typical of PM products.

3.5 Flexural properties of sintered materials

Representative examples of load-displacement curves obtained from the three points bending tests for Ti32-BE and Ti32-MA samples are shown in Figure 6 a) and Figure 6 b), respectively. In particular, a comparison of the curves for constant processing time (2h: 1250ºC vs. 1350ºC) and same sintering temperature (1250ºC: 2h vs. 4h) are shown. Analysing the curves of Figure 6, it can be noted that, generally, the lower the processing temperature the higher the load withstood and the greater the toughness with the only exception of the Ti32-BE samples sintered at 1250ºC for 2 hours. This exemption is mainly due to the lower relative density of Ti32-BE specimens with respect to the other materials. Ti32-BE and Ti32-MA components show very similar mechanical behaviour which seems not to be influenced by the processing parameters. Specifically, the materials undergo elastic deformation up to approximately 1200 N of load prior to reach the plastic deformation region. In opposition, the amount of plastic deformation is greatly influenced by the sintering condition and the load at rupture is lower than the maximum load. The curves shown in Figure 6 overlap in the elastic region, therefore, indicating that the flexural modulus is constant. The elastic modulus determined by means of three points bending tests on Ti32-BE and Ti32-MA specimens is not reported because does depend on the span length to diameter ratio [23, 24] and , therefore, is not a characteristic of the materials studied.

As indicated in the experimental procedure, the elastic limit values were measured by means of the off-set method and their variation as a function of the sintering temperature is presented in Figure 7.

From Figure 7, the elastic limit of Ti32-BE samples decreases a little with the sintering temperature. The only exception are the Ti32-BE specimens sintered at 1250ºC-2h which have lower elastic limit but much higher standard deviation (1080 ± 104 MPa). Moreover, the processing time does not have a significant effect on the elastic limit of Ti32-BE components. The low elastic limit of the samples sintered at 1250ºC-2h is due to the higher volume percentage of residual porosity (i.e. higher number of crack-initiation or stress-concentration sites). For the other processing conditions studied it seems that the effect of the reduction of the residual porosity is overcome by the effect of the grain growth which takes place when the sintering temperature is increased or the dwell time is prolonged and the increment of the amount of interstitials. In the case of the Ti32-MA samples, the elastic limit remains almost constant at 1200 MPa with the exception of the samples sintered at 1250ºC-2h and at 1350ºC-4h whose elastic limit mean value is a little bit higher although their standard deviation is greater. Therefore, in the case of the Ti32-MA specimens the elastic limit is the result of the equilibrium of the effects of the level of relative density, amount of interstitial elements and features of the microconstituents. When comparing the powder production method, Ti32-BE samples have relatively higher elastic limit with respect to the Ti32-MA specimens except for the samples processed at 1250ºC-2h. This result is mainly due to the compromise between the higher relative density, lower amount of interstitials and coarser microstructure of Ti32-MA with respect to Ti32-BE. Finally, the data shown in Figure 7 are higher than those available in the literature for biomedical products (wrought Ti-6Al-4V: 903-1090 MPa) [25] due to the compromise between residual porosity, amount of oxygen and finer microstructural features of PM Ti-3Al-2.5V samples in comparison to wrought materials.

The variation of the flexural strain (ε_f) as a function of the sintering parameters for Ti32-BE and Ti32-MA samples is shown in Figure 8.

From the data plotted in Figure 8, the flexural strain of Ti32-BE samples decreases with the increasing of the sintering temperature, independently of the processing times considered. Because the reduction of the residual porosity should lead to a higher strain, this decreasing trend is due to the combined effect of the increment of the amount of interstitials dissolved by the alloy which increases with the increment of the processing temperature and the coarsening of the microstructure. From the data of the flexural strain of the Ti32-BE samples, generally, longer processing time leads to a higher ductility. The only exception to this trend are the samples sintered at 1250ºC-2h which have by the lowest value of flexural strain due to lower level of relative density that these samples have. As for the Ti32-BE samples, the flexural strain of Ti32-MA specimens decreases with the increment of the sintering time. From the comparison of the flexural strain data as a function of the way to add the alloying elements, Ti32-MA samples always have higher strain in comparison to Ti32-BE specimens. The higher strain of the Ti32-MA samples is the compromise between the lower residual porosity (i.e. less crack initiation or stress concentration sites), lower amount of interstitials and coarser microstructure in comparison to the Ti32-BE specimens.

The results of the fractographic study of the Ti32-BE and Ti32-MA samples sintered using diverse processing temperatures are shown in Figure 9.

From the fractographic study results (Figure 9), in general the rupture of the Ti-3Al-2.5V samples sintered in the processing temperature range between 1250-1350ºC occurs by the separation of the grain boundaries, typical of the inter-crystalline rupture, even though the presence of river-marking inside the grains is due to trans-crystalline rupture where this last one becomes more important at higher temperatures or longer times. Moreover, dimples form from the residual pores and are visible in the micrographs. The rupture mode is in agreement

with the results of the load-displacement curves shown in Figure 6 and it is a typical cleavage rupture of metals with hexagonal lattice.

3.6 Thermal conductivity and electrical resistivity of sintered materials

The values of the thermal conductivity and of the electrical resistivity for the specimens sintered under various temperature-time conditions are reported in Table 3.

From Table 3, the thermal conductivity values for Ti32-BE samples lay between 8.0 W/m·ºC and 8.2 W/m·ºC and, consequently, the variation found is not that significant. This seems to indicate that the thermal conductivity at room temperature of Ti32-BE specimens is not greatly influenced by the microstructural features and to the fact that the relative density is just a bit higher than 92%. This limited variation could be the compromise between the relative density (or on the contrary the amount of residual porosity with dissimilar size and distribution), the microconstituents (α and β) and the total amount of interstitials. In the case of the Ti32-MA components, the thermal conductivity at room temperature (Table 3) increases with the increment of the relative density (i.e. sintering temperature) for 2 hours of processing time. This is most probably due that the effect of lowering the residual porosity and grain growth induced by the increment of the temperature overcomes the effect of the interstitial elements. When considering the data for the components sintered at 4 hours, the thermal conductivity is almost constant but then drops suddenly. Apart from the value measured on the specimens sintered at 1350ºC-4h, the variation of the thermal conductivity at room temperature of Ti32-MA samples is limited, since the values range between 8.9 W/m·ºC and 9.3 W/m·ºC. Comparing the method to fabricate the powder, Ti32-MA specimens have always a greater thermal conductivity than Ti32-BE samples. This can be explained on the bases of the greater relative density, lower oxygen and bigger grain size of Ti32-MA components with respect to Ti32-BE samples. With respect to the conventional value of thermal conductivity indicated for this alloy, generally, k measured in products

fabricated from Ti32-BE and Ti32-MA powders results to be directly comparable or somewhat higher, respectively. Analysing the electrical resistivity data for the Ti32-BE components (Table 3), this property decreases for 2 hours and increases for 4 hours of dwell time but this variation is not very important since the values range between 142 and 146 μΩ·cm. Possibly, this is due to the equilibrium between relative density, interstitials and microstructural features as in the case of the thermal conductivity. In opposition to the Ti32-BE samples, the trends of the electrical resistivity for the Ti32-MA specimens (Table 3) always increases a bit but, as in the case of the Ti32-BE alloy, the variation of the resistivity with the various sintering conditions is not that significant. The only exceptions are the products sintered at 1350ºC-4h which have a higher resistivity. Comparing the alloying elements addition method, Ti32-MA specimens have lower electrical resistivity than Ti32-BE samples, which is equivalent to a higher electrical conductivity. This behaviour could have been expected due to the higher thermal conductivity found in the Ti32-MA alloy owed to the higher relative density of these components. With respect to the value of electrical resistivity of the wrought alloys (see Table 3), Ti32-MA samples have very similar electrical resistivity even though of the higher amount of interstitials and the presence of the residual porosity while Ti32-BE specimens have higher resistivity most probably due to the lower relative density and to the relatively higher equivalent oxygen with respect to Ti32-MA samples.

The thermal conductivity as a function of the temperature was measured in Ti32-BE and Ti32-MA specimens sintered at 1250ºC for 2 hours and the results are presented in Figure 10. From the thermal conductivity of pressing and sintering Ti-3Al-2.5V components data shown in Figure 10, this property increases with the temperature independently of the PM method used to add the alloying elements. The increasing trend is due to the greater mobility of electrons and phonons throughout the lattice with the increment of the temperature. When considering the method to fabricate the alloy, Ti32-MA samples have higher thermal conductivity, as it was for the thermal conductivity at room temperature (Table 3), due to the

higher relative density. As expected, when the effect of the temperature on the C_p value is considered, the thermal conductivity of the materials is higher. With respect to wrought Ti-3Al-2.5V alloy [3], the values, either measured or calculated, of the Ti32-BE specimens are always lower, whilst the measured values of Ti32-MA samples are higher up to 100ºC and the calculated ones up to 180ºC than the wrought alloy. Moreover, the ratio at which the thermal conductivity of the wrought alloys increases with the temperature is greater than the pressed and sintered products due to the presence of the residual porosity.

4. Conclusions

This study demonstrated that it is possible to obtain sintered Ti-3Al-2.5V products with relative density variable between 94% and 97% and with homogeneous microstructures starting from HDH powder and, thus, avoiding the inconvenient of the presence of the chlorides. Because of this, the blending elemental method is a suitable way to replace, normally, more costly pre-alloyed powders. PM Ti-3Al-2.5V samples show similar mechanical properties to that of the wrought alloy; however, the ductility is lowered due to the residual porosity and the relatively high amount interstitials dissolved. Moreover, thermal conductivity and electrical resistivity values similar to those of the wrought alloy by processing the Ti-3Al-2.5V alloy by means of pressing and sintering.

5. Acknowledgements

The financial support from the Spanish Ministry of Science through the R&D Projects MAT2009-14448-C02-02 and MAT2009-14547-C02-02, and from Regional Government of Madrid through the ESTRUMAT (S2009/MAT-1585) project is acknowledged. The possibility to perform the measurements of the thermal conductivity and electrical resistivity in the Fraunhofer IFAM-Dresden Institute is really appreciated.

6. References

[1] Lütjering G, Williams JC. Titanium - Engineering Materials and Processes. 1st ed. Manchester: Springer; 2003.

[2] Leyens C, Peters M. Titanium and Titanium Alloys. Fundamentals and Applications. Köln: Wiley-VCH; 2003.

[3] Boyer R, Welsch G, Collings EW. Materials Properties Handbook - Titanium Alloys. Ohio: ASM International; 1998.

[4] German RM. Powder Metallurgy of Iron and Steel. New York: Wiley; 1998.

[5] Hurless BE, Froes FH. Lowering the Cost of Titanium. AMPTIAC Quarterly 2002;6:3-10.

[6] Welsch G, Lee Y-T, Eloff PC, Eylon D, Froes FH. Deformation Behaviour of Blended Elemental Ti6Al4V Compacts. Metall. Mater. Trans. A 1983;14:761-9.

[7] Froes FH, Eylon D. Powder Metallurgy of Titanium Alloys - A Review. Powder Metall. Internat. 1985;17:163-7.

[8] Froes FH, Eylon D. Powder Metallurgy of Titanium Alloys - A Review. Powder Metall. Internat. 1985;17:235-8.

[9] Songsiri K, Manonukul A, Chalermkarnnon P, Nakayama H, Fujiwara M. Effects of Sintering Temperature and Sintering Time on Mechanical and Impact Properties of Injection Moulded Ti-6Al-4V Employing Pre-alloyed and Mixed Powders. In: Lawcock R, Lawley A, McGeehan PJ editors. Advances in Powder Metallurgy & Particulate Materials, Washington D.C.: MPIF; 2008, p. 175-82.

[10] Wang L, Lang ZB, Shi HP. Properties and Forming Process of Pre-alloyed Powder Metallurgy Ti6Al4V Alloy. Trans. Non-Ferrous Met. Soc. China 2007;17:s639-s43.

[11] Ivasishin OM, Eylon D, Bondarchuk VI, Savvakin DG. Diffusion during Powder Metallurgy Synthesis of Titanium Alloys. Defect and Diffusion Forum 2008; 277:177-85.

[12] Sun F, Yu KOO. Development of Cost-Effective Blended Elemental Powder Metallurgy Ti Alloys, In: Gungor MN, Ashraf Imam M, Froes FH, editors. Innovations in Titanium Technology, New York: Wiley; 2007, p. 19-27.

[13] Druz VA, Moxson VS, Chernenkoff R, Jandeska WF Jnr, Lynn J. Blending an Elemental Approach to Volume Titanium Manufacture. Metal Powder Report 2006;61:16-21.

[14] Bolzoni L, Esteban PG, Ruiz-Navas EM, Gordo E. Influence of Powder Characteristics on Sintering Behaviour and Properties of P/M Ti Alloys Produced from Pre-alloyed Powder and Master Alloy. Powder Metall. 2011;54:543-50.

[15] van der Pauw LJ. A Method of Measuring Specific Resistivity and Hall Effect of Discs of Arbitrary Shape. Philips Res. Reports 1958;13:1-9.

[16] van der Pauw LJ. A Method of Measuring Specific Resistivity and Hall Effect on Lamellae of Arbitrary Shape. Philips Tech. Review 1958;20:220-4.

[17] Ivasishin OM, Anokhin VM, Demidik AN, Savvakin DG. Cost-effective Blended Elemental Powder Metallurgy of Titanium Alloys for Transportation Application. Key Eng. Mater. 2000;188:55-62.

[18] Ivasishin OM. Cost Effective Manufacturing of Titanium Parts with Powder Metallurgy Approach. Mater. Forum 2005;29:1-8.

[19] Bolzoni L, Esteban PG, Ruiz-Navas EM, Gordo E. Mechanical Behaviour of Pressed and Sintered Titanium Alloys Obtained from Master Alloy Addition Powders. J. Mech. Behav. Biomed.l Mater. 2012;15:33-45.

[20] Jaffee RI, Campbell IE. The Effect of Oxygen, Nitrogen and Hydrogen on Iodide-refined Titanium. Trans. Am. Inst. Mining and Metall. Eng. 1949;185:646-54.

[21] Jaffee RI, Ogden HR, Maykuth DJ. Alloys of Titanium with Carbon, Oxygen and Nitrogen. Trans. Am. Inst. Mining and Metall. Eng. 1950;188:1261-6.

[22] Finlay WL, Snyder JA. Effects of Three Interstitial Solutes (Nitrogen, Oxygen and Carbon) on the Mechanical Properties of High-purity Alpha Titanium. J. of Metals 1950:188:277-86.

[23] Alander P, Lassila LVJ, Vallittu PK. The Span-length and Cross Sectional Design Affect Values of Strength. Dental Mater. 2005;21:347-53.

[24] Stewardson DA, Shortall AC, Marquis PM, Lumley PJ. The Flexural Properties of Endodontic Post Materials. Dental Mater. 2010;26:730-6.

[25] Henry D. Materials and Coatings for Medical Devices - Cardiovascular. Ohio: ASM International; 2009.

Table 1. Morphology, particle size and amount of interstitials of Ti32-BE and Ti32-MA powders.

Material	*Ti32-BE*	*Ti32-MA*
Morphology	Irregular	Irregular
D_{50}[µm]	38.79	39.00
D_{90} [µm]	74.65	79.65
Oxygen [wt.%]	0.402	0.337
Nitrogen [wt.%]	0.0101	0.0118

Table 2. Amount of interstitials as a function of the sintering conditions for Ti32-BE and Ti32-MA samples.

Material	**Processing conditions**	**Interstitials**	
		Oxygen [wt.%]	*Nitrogen [wt.%]*
Ti32-BE	1250ºC-2h	0.42 ± 0.02	0.017 ± 0.001
	1300ºC-2h	0.40 ± 0.01	0.019 ± 0.001
	1350ºC-2h	0.45 ± 0.03	0.021 ± 0.003
	1250ºC-4h	0.40 ± 0.01	0.020 ± 0.002
	1300ºC-4h	0.43 ± 0.07	0.020 ± 0.001
	1350ºC-4h	0.49 ± 0.02	0.024 ± 0.001
Ti32-MA	1250ºC-2h	0.34 ± 0.01	0.020 ± 0.002
	1300ºC-2h	0.35 ± 0.01	0.020 ± 0.001
	1350ºC-2h	0.38 ± 0.02	0.023 ± 0.003
	1250ºC-4h	0.35 ± 0.01	0.016 ± 0.005
	1300ºC-4h	0.36 ± 0.02	0.018 ± 0.002
	1350ºC-4h	0.40 ± 0.02	0.023 ± 0.001

Table 3. Thermal conductivity and electrical resistivity for Ti32-BE and Ti32-MA sintered samples.

Material	**Processing conditions**	**Property**	
		Thermal Conductivity [W/m·K]	*Electrical Resistivity [μΩ·cm]*
Ti32-BE	1250ºC-2h	8.10	146.0
	1300ºC-2h	8.00	145.4
	1350ºC-2h	8.04	144.2
	1250ºC-4h	8.16	142.4
	1300ºC-4h	8.18	145.2
	1350ºC-4h	8.12	145.2
Ti32-MA	1250ºC-2h	8.97	128.8
	1300ºC-2h	8.90	133.7
	1350ºC-2h	9.13	132.3
	1250ºC-4h	9.26	130.1
	1300ºC-4h	9.25	133.2
	1350ºC-4h	8.23	142.6
Ti-3Al-2.5V	Wrought	8.30	126.0

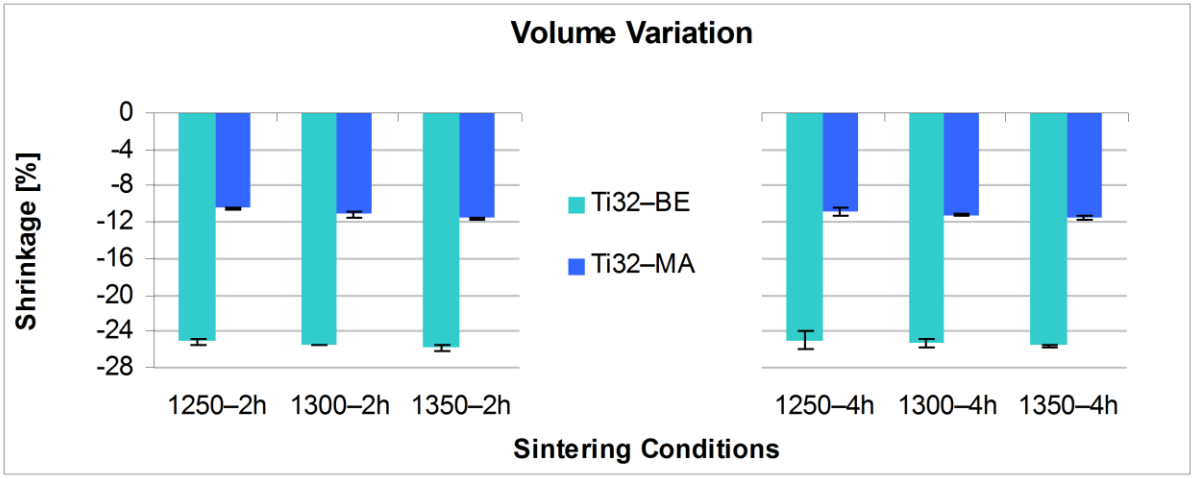

Fig. 1

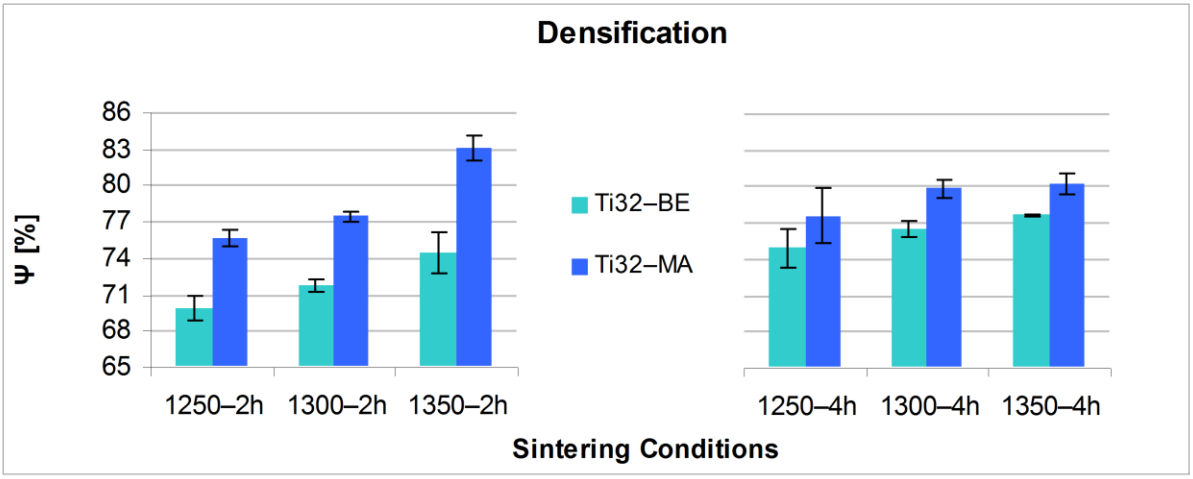

Fig. 2

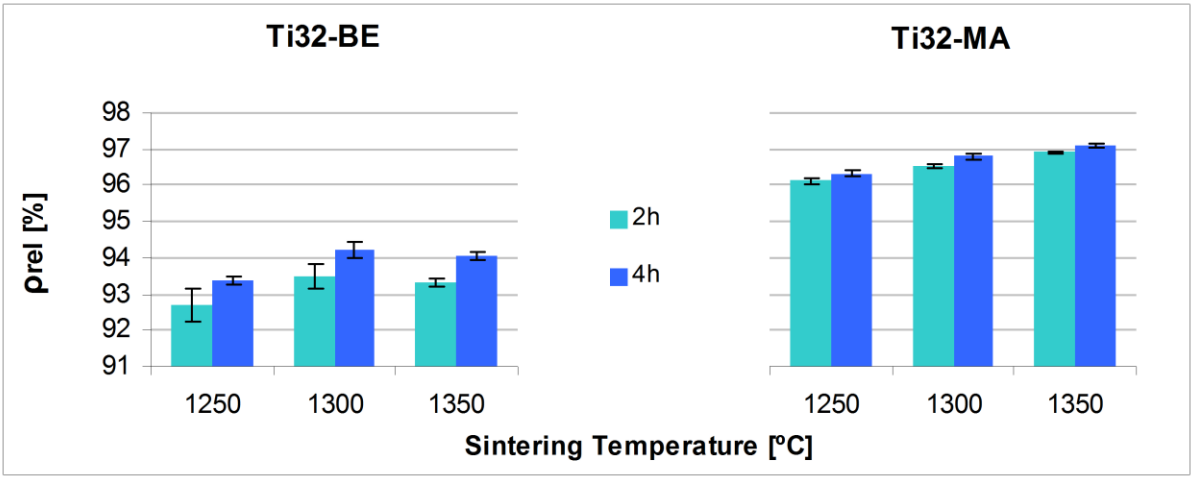

Fig. 3

Figure 4. Representative micrograph of samples sintered at 1250ºC-2h: a) Ti32-BE and b) Ti32-MA, at 1350ºC-2h: c) Ti32-BE and d) Ti32-MA and at 1250ºC-4h: e) Ti32-BE and f) Ti32-MA.

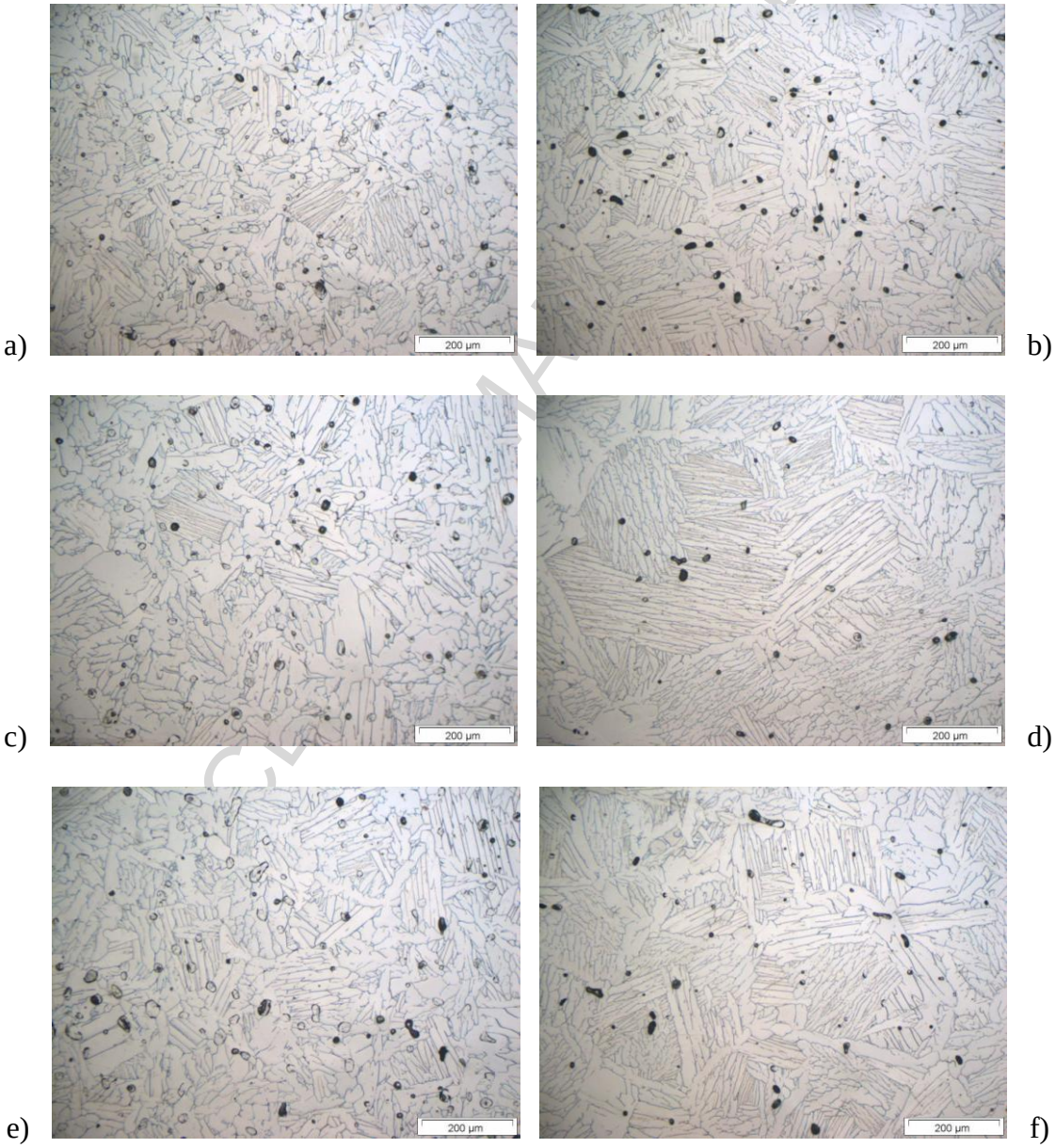

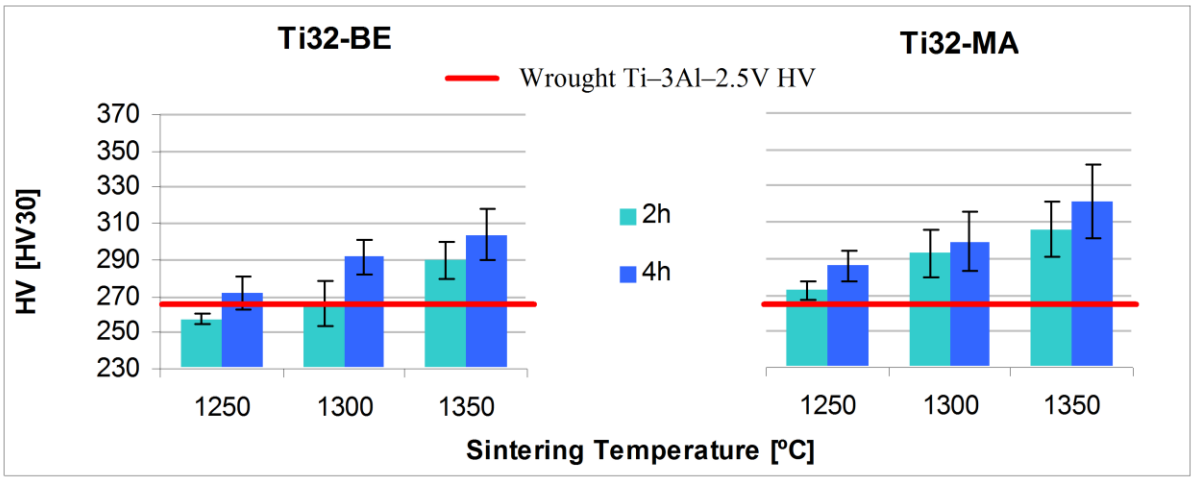

Fig. 5

Figure 6. Representative load-deflection curves of sintered samples: a) Ti32-BE and b) Ti32-MA.

a)

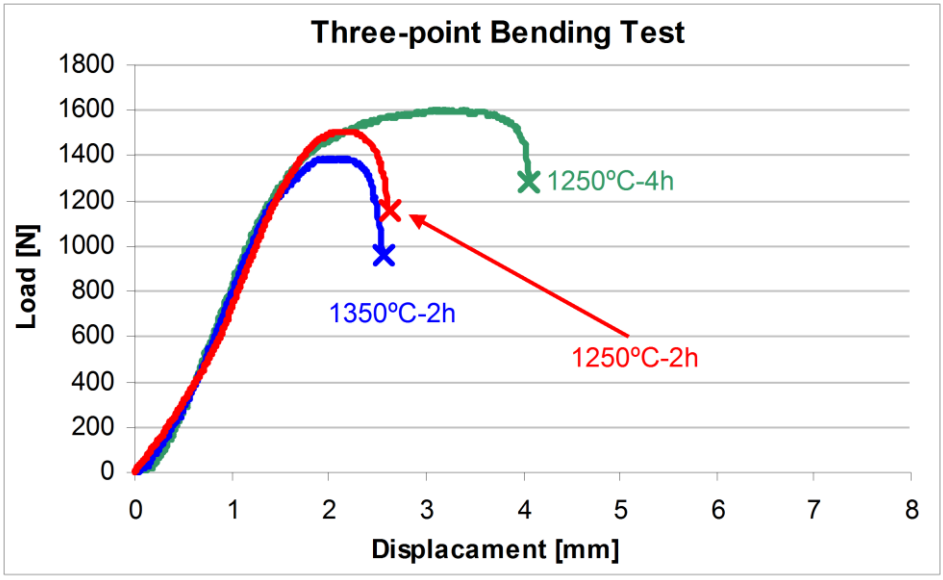

b)

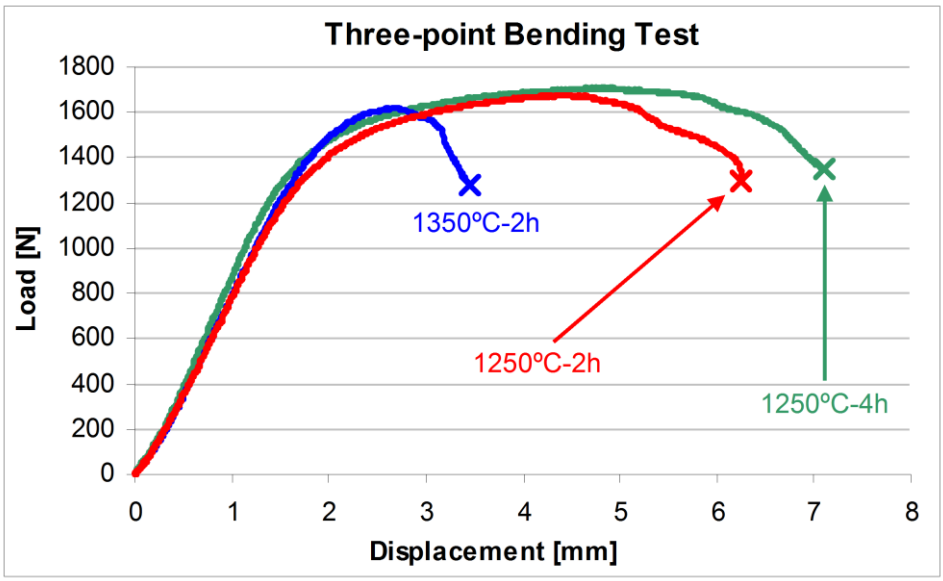

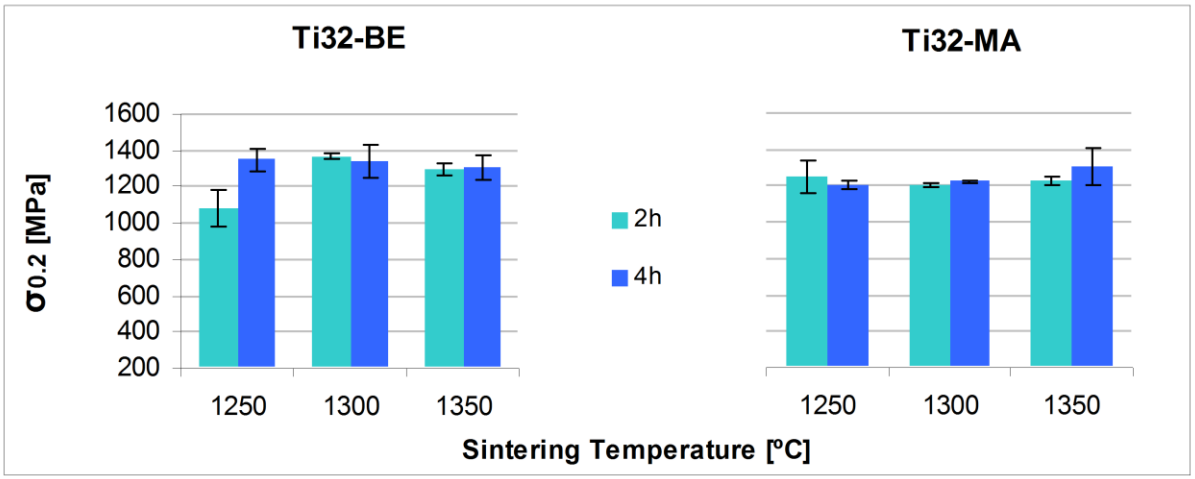

Fig. 7

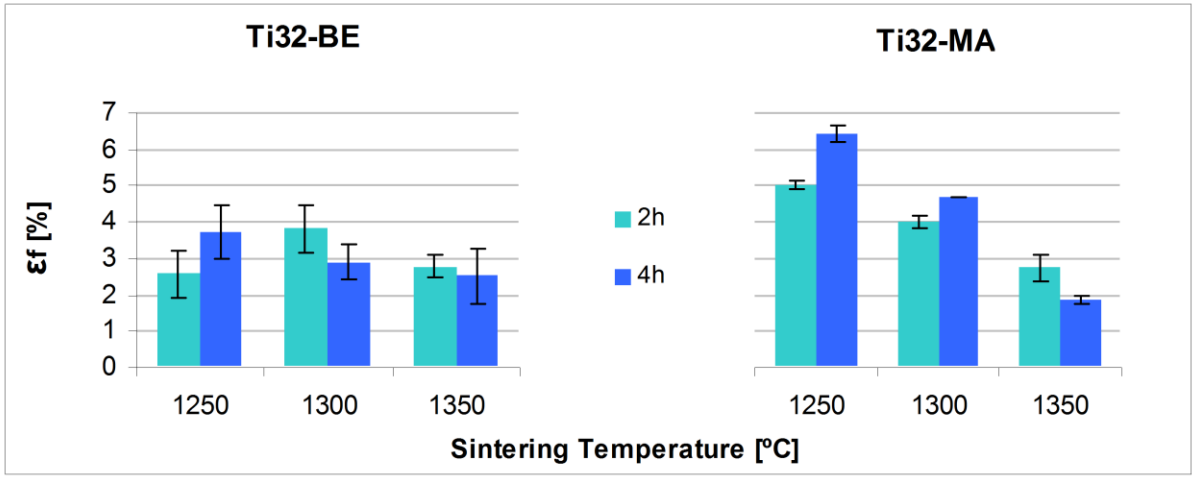

Fig. 8

Figure 9. Fracture surface of the samples sintered at 1250ºC-2h: a) Ti32-BE and b) Ti32-MA, at 1350ºC-2h: c) Ti32-BE and d) Ti32-MA and at 1250ºC-4h: e) Ti32-BE and f) Ti32-MA.

a) 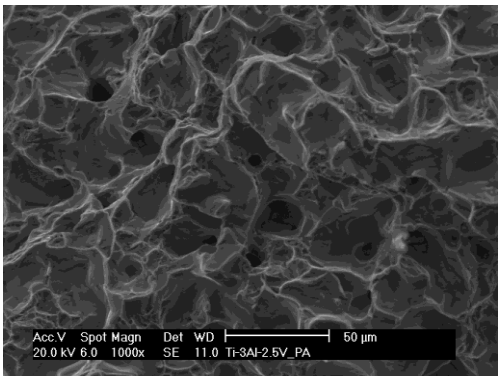

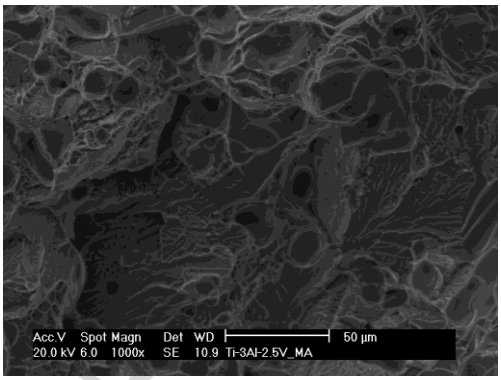

b)

c) 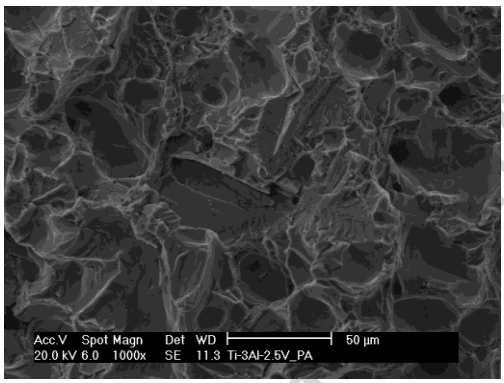

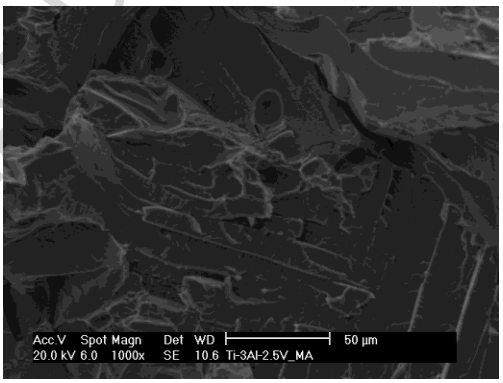

d)

e) 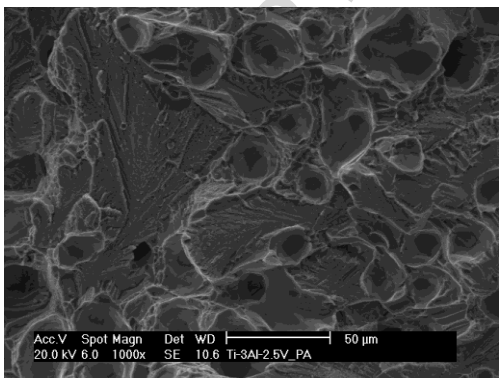

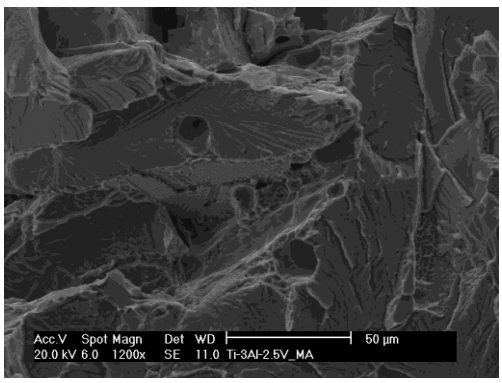

f)

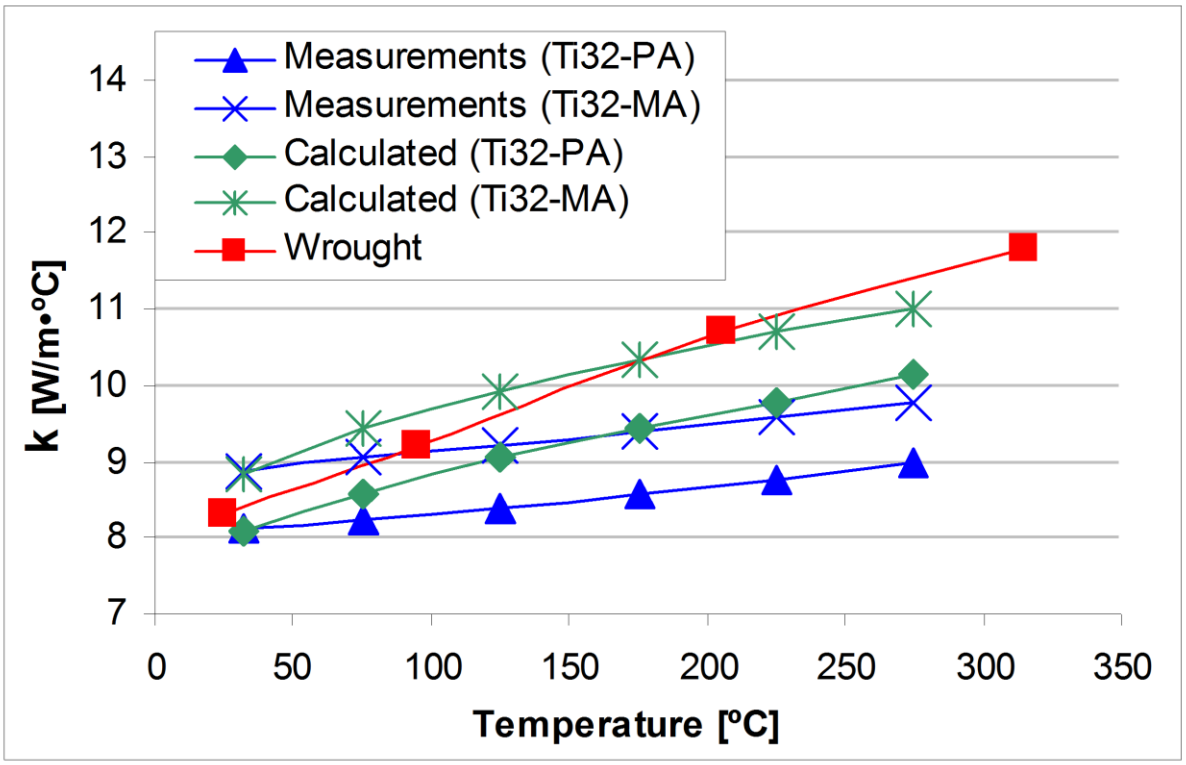

Fig. 10

Figure 1. Volume variation as a function of the sintering conditions for Ti32-BE and Ti32-MA sintered samples.

Figure 2. Densification as a function of the sintering conditions for Ti32-BE and Ti32-MA sintered samples.

Figure 3. Relative density as a function of the sintering conditions for Ti32-BE and Ti32-MA sintered samples.

Figure 4. Representative micrograph of samples sintered at 1250ºC-2h: a) Ti32-BE and b) Ti32-MA, at 1350ºC-2h: c) Ti32-BE and d) Ti32-MA and at 1250ºC-4h: e) Ti32-BE and f) Ti32-MA.

Figure 5. Variation of the hardness as a function of the sintering temperature for Ti32-BE and Ti32-MA sintered samples.

Figure 6. Representative load-displacement curves of sintered samples: a) Ti32-BE and b) Ti32-MA.

Figure 7. Variation of the elastic limit as a function of the sintering temperature for Ti32-BE and Ti32-MA sintered samples.

Figure 8. Variation of the strain at rupture as a function of the sintering temperature for Ti32-BE and Ti32-MA sintered samples.

Figure 9. Fracture surface of the samples sintered at 1250ºC-2h: a) Ti32-BE and b) Ti32-MA, at 1350ºC-2h: c) Ti32-BE and d) Ti32-MA and at 1250ºC-4h: e) Ti32-BE and f) Ti32-MA.

Figure 10 - Thermal conductivity as a function of temperature for Ti32-BE and Ti32-MA specimens.

Highlights

> Blending elemental and master alloy addition powders are used to fabricate titanium alloys. > The effect of sintering parameters on the final properties is evaluated. > Flexural properties of powder metallurgy Ti-3Al-2.5V alloy are asserted.> Thermal conductivity and electrical resistivity of PM Ti-3Al-2.5V materials are determined.